



# Development of Biomimetic Hydroxyapatite Containing Dental Restorative Composites

Aysu Aydınoglu<sup>1</sup> · Jülide Hazal Türkcan<sup>1</sup> · Ergün Keleşoğlu<sup>2</sup> · Afife Binnaz Hazar Yoruç<sup>1</sup>

Received: 9 May 2021 / Accepted: 30 January 2022 / Published online: 25 February 2022  
© King Fahd University of Petroleum & Minerals 2022

## Abstract

The aim of the study was to evaluate the incorporation effect of biomimetic hydroxyapatite (BHA) particles on the mechanical properties of experimental dental composites. Two experimental composites were produced from the same organic matrix, Si/Zr nanocluster, and SiO<sub>2</sub>/silane as main inorganic reinforcing fillers. 7wt% BHA was added to one of the groups to evaluate its effect on mechanical properties. The BHA was also modified with 3-MPTMS to improve chemical bonding. Chemical structures and physical properties of the fillers were identified by XRD, FTIR, XPS, TGA, SEM, BET, and Zeta-Sizer. According to ISO 4049 and DIN 50,133 the mechanical properties, and to ISO 10993–5:2009 the biocompatibility was investigated. Analysis of variance (ANOVA) was used for the statistical analysis of acquired data. The BHA was synthesized by the biomimetic method in simulated body media (SBF). The SEM images of BHA/Silane particles demonstrated rod-like shapes and similar dimensions with natural hydroxyapatite present in tooth enamel. The modification by using 3-MPTMS was decreased the mean particle size of the fillers due to a lower agglomeration tendency. Moreover, the addition of small mass fractions of the BHA into the dental resins can substantially meet the ISO 4049 requirements. Consequently, the BHA was not adversely decreasing the mechanical properties of the dental composites. Also, the biocompatibility of the BHA-containing composites was found better than the samples without BHA-containing composites. The incorporation of the BHA can meet the mechanical requirements of dental resins and composites. Additionally, it may show regenerative properties against small lesions.

**Keywords** Biomimetic hydroxyapatite · Silanization · Dental composite · Mechanical properties · In vitro cytotoxicity

## 1 Introduction

Health problems such as fractures, abscesses, and caries in the oral environment decrease the quality of life and affect aesthetics negatively [1]. Because of its progressive property, early diagnosis and treatment of the caries are extremely important and thus, interest in composite fillings has increased due to their aesthetics, biocompatibility, ease of application, and favorable mechanical properties [2, 3]. The most commonly used monomers are urethane dimethacrylate (UDMA), bisphenol-A glycidyl methacrylate (Bis-GMA), 2-Hydroxyethyl methacrylate (HEMA), triethylene glycol

dimethacrylate (TEGDMA), and ethoxylated bisphenol-A dimethacrylate (BisEMA) [4]. Nevertheless, inorganic fillers generally made of finely divided silicate and glass particles such as borosilicate glasses or colloidal silica, are combined to enhance inadequate properties of these organic phases [5]. Moreover, calcium phosphate-based ceramics such as hydroxyapatite (HA), amorphous calcium phosphate, tetra-calcium phosphate, and mono- and dicalcium phosphate, are used as inorganic fillers to provide calcium and phosphate released from dental composites [6]. Among them, the HA has considered as a good candidate thanks to its biological and mechanical properties, similarity with mammals teeth and bones, radio-opacity, moisture resistance, and hardness [7]. Additionally, the HA can provide remineralization and prevent demineralization. [8]. There are many HA particles with various shapes such as spheres, fibers, rods, and wires from the micro to the nanoscale. In the literature, different HA particles were used in dental composites [9–11]. Among

✉ Aysu Aydınoglu  
aysuaydn@yildiz.edu.tr

<sup>1</sup> Department of Metallurgical and Materials Engineering, Yildiz Technical University, 34210 Istanbul, Turkey

<sup>2</sup> Faculty of Science, Materials Science and Technologies, Turkish-German University, 34820 Istanbul, Turkey



them, with the usage of nanotechnology in dentistry, nano-sized particles synthesized by biomimetic methods have gained importance in restoratives [12]. Recently, nanostructured biomimetic hydroxyapatite (BHA), which can protect the teeth with the formation of a new layer of synthetic enamel, are extensively searched for dental composites [13, 14]. However, low fracture toughness, inadequate tensile strength, and brittleness restrict their individual usage as a filler in restoratives. Therefore, these materials were usually used with the other filler particles such as silica and Si/Zr nanoclusters that better mimic the appearance of natural teeth due to their opalescence [15–17].

The silanization process can also provide homogenous dispersion of the particles in the viscous organic matrix and improve mechanical properties [18, 19]. Our previous study proved that silanization by using methacryloxy silane-based agent improves mechanical properties of the dental restorative materials [20].

50–70% of restorations fail because of secondary caries formation due to the plaque-causing bacterias such as *streptococcus mutans* (*S.Mutants*), *streptococcus aeurus* (*S.Aeurus*), and lactobacilli [21–23]. Therefore it is very important to prevent biofilm formation and gain regenerative properties to composite in order to heal natural tissue. As it was proved HA has good bioactivity and it prevents biofilm formation on the surfaces as a ceramic block [24]. Thus, it is expected that the use of HA as a filler in composites can also prevent the formation of biofilm (plaque) on the composite surfaces [25]. However, the most important point is that HA added composites should meet the requirements given in ISO 4049.

In this study, according to our knowledge biomimetic hydroxyapatite (BHA) has been used as an inorganic filler in dental composites for the first time and, evaluated in the scope of mechanical, chemical, physical, and biological properties.

## 2 Materials and Methods

### 2.1 Materials

UDMA ( $\geq 97\%$ ), Bis-GMA ( $> 98\%$ ), Bis-HEMA ( $\geq 97\%$ ), TEGDMA ( $> 95\%$ ), camphorquinone (CQ,  $> 97\%$ ), ethyl-4-dimethylaminobenzoate (4-EDMAB,  $\geq 99\%$ ), 3-MPTMS ( $> 98\%$ ), zirconyl acetate solution ( $Zr^{x+} \cdot xCH_3COOH$ ) and colloidal silica solution (Ludox®, average particle size 40 nm) were obtained from Sigma-Aldrich, Germany. All materials were of analytical grade and used as received without further purification.

**Table 1** Composition of the experimental dental composites

Sample Code	Reinforced Fillers	% (wt)
C1	SiO <sub>2</sub> /silane	35
	Si/Zr nanocluster/silane	35
C2	SiO <sub>2</sub> /silane	31.5
	Si/Zr nanocluster/silane	31.5
	BHA/silane	7

### 2.2 Synthesis of Reinforced Fillers

The BHA was synthesized by using the co-precipitation technique in simulated body fluids (SBF) according to our previous study [26]. The SBF was prepared according to Taş's recipe that is similar to human blood plasma [27]. SiO<sub>2</sub> reinforced fillers were obtained from commercial colloidal silica solution Ludox HS-40. At first, Ludox HS-40 was dried at 80 °C. Then, powders were grained with a ball mill for one day. Finally, grained powders were sieved from 250 meshes (63 μm). The pH value of the colloidal silica solution (500 ml) was adjusted to 2.5 with diluted HNO<sub>3</sub>. This solution was added slowly to Zr<sup>x+</sup>·xCH<sub>3</sub>COOH (230.65 ml) and mixed for one hour. The mixture was dried at 80 °C and then calcined at 550 °C for 4 h in a furnace. Calcined Si/Zr powders were grained with ball mill for one day and then sieved from 450 meshes (32 μm). The BHA, SiO<sub>2</sub> ve Si/Zr nanocluster were modified with 3-MPTMS. The BHA synthesis, SBF preparation, and silanization process are described in detail in our previous study [28].

### 2.3 Preparation of Dental Composites

BisGMA (4.5% wt.) was stirred for 10 min at 40 °C in an ultrasonic water bath, then HEMA (10% wt.), UDMA (10% wt.), and TEGDMA (4.5% wt.) were added to the BisGMA. The synthesized filler (70% wt.) was added to the organic matrix and, stirred for one day in the ultrasonic water bath to obtain homogenous dispersion. Camphorquinone (0.2% wt.) and 4-EDMAB (0.8% wt.) were added to the composite and stirred for 3 h. Finally, the resins were kept in the vacuum oven at 37 °C for 30 min to remove air bubbles. The ratios of inorganic phases in dental composites are given in Table 1.

### 2.4 Characterization of Fillers

The mineralogical structures, purity, and crystallization degree of the fillers were determined by X-Ray Diffractometer (MiniFlex 300/600, Rigaku RD). 2θ area was scanned by X-Rays that obtained by using Cu-Kα radiation (1.54059 Å) with 0.02° distances and scan rate of 0.5 s/min. Fourier transform infrared spectroscopy (FTIR) was performed to observe

the bonding of the filler and 3-MPTMS. For the sample preparation, the fillers were dried at 80 °C, mixed with powdery KBr, and pelletized under pressure. The spectra were recorded in the range of 1300 to 400  $\text{cm}^{-1}$  with a resolution of 4  $\text{cm}^{-1}$  by using the FTIR device (Spectrum One, Perkin Elmer 2000). To determine binding properties of the silica and 3-MPTMS, silanized silica fillers were analyzed by X-Ray photoelectron spectroscopy (XPS) (EA 300 and SPECS devices) et al. monochromatic mode and 57 W power. Thermogravimetric analysis (TGA) (Rigaku Thermal Analyzer) was performed to determine relative amounts of organic and inorganic structures. The measurement was carried out under air conditions with a heating rate of 10 °C/min from 50 to 900 °C. The surface morphology of silanized/unilanized fillers was examined with the scanning electron microscope (SEM, JSM 5600, Jeol) by using 10 kV energy. Before the analysis, the samples were coated with 20–30 nm gold in order to ensure conductivity. The particle size distribution of the fillers was obtained by using the light scattering technique with Zeta-Sizer (Nano ZS, Malvern). Surface area measurements were performed by using the BET (Autosorb-6B, Quantochrome) device.

## 2.5 Characterization of Dental Composites

### 2.5.1 Determination of Mechanical Properties

Compressive strength (CS), flexural strength (FS), and modulus of elasticity (E) were determined using a universal testing machine (custom-made, Devotrans) according to ISO 4049. In order to determine the CS, five samples were prepared using 6 mm height  $\times$  4 mm diameter cylindrical teflon mold and cured on both sides with a blue-LED light device (Eli-par™ S10, 3 M ESPE) for 20 s. The five specimens of each group were stored at 37 °C in distilled water for 7 days and dried at 37 °C for 1 day before testing [29, 30]. The CS of the composites were calculated using Eq. 1:

$$\sigma_c = F/A \quad (1)$$

$\sigma_c$ : The compressive strength (MPa),  $F$ : Maximum force (N) applied at fracture formation,  $A$ : Cross-sectional area ( $\text{mm}^2$ ) of the sample

Five bar-shaped specimens (25 mm length  $\times$  2 mm height  $\times$  2 mm wide) were prepared for each experimental dental composite for flexural strength, and elastic modulus according to the ISO 4049. After storage in distilled water at 37 °C for 24 h, the specimens were submitted to a three-point bending test in a universal testing machine (Custom made). The FS (Eq. 2) and E (Eq. 3) were calculated by using mean values of five measurements of each group [29].

$$\sigma_b = 3Fl/(2bd^2) \quad (2)$$

$\sigma_b$ : Flexural strength (MPa),  $F$ : Maximum force (N) applied at fracture formation,  $l$ : Distance between supports (20 mm),  $b$ : Width of the sample (mm),  $d$ : Thickness of the sample (mm)

$$E = (Fl^3)/(4bh^3d) \quad (3)$$

$E$ : Modulus of elasticity (GPa),  $F$ : Maximum force applied before plastic deformation (N),  $l$ : Distance between supports (20 mm),  $b$ : Width of the sample (mm),  $d$ : Thickness of the sample (mm),  $h$ : Dimension changes of the sample (mm).

Vicker's hardness (VH) of the composites was determined according to DIN 50,133. For the test 3 samples were prepared in a diameter of 19  $\times$  2 mm cylindrical teflon mold. Before testing, cured samples were placed in distilled water at 37 °C for 28 days and dried. The surface was ground with the 1000 grid abrasion paper before testing. The VH of the dried samples was determined with a nanoindentation test device (CSM Instruments', UNHT) with a loading of 0.5 kg for 60 s. The average value for each group was calculated.

### 2.5.2 Determination of Biological Properties

The biocompatibility of the composites was evaluated according to ISO 10993–5:2009. In vitro cytotoxicity of the dental composites was determined by using L929 cells (ATCC CLL 1; American Type Culture Collection, Rockville, MD) recommended in the relevant standard and cell viability (CV %) of the composites was calculated.

### 2.6 Statistical Analysis

Normality of the mechanical test results was determined by Kolmogorov–Smirnov test for Flexural Strength, Elastic Modulus Compressive Strength, and Vickers Hardness. Student t-test was performed with SPSS (SPSS Inc., version 21.0; Chicago, USA). In all the statistical evaluations,  $p < 0.05$  was regarded as significant,  $p < 0.01$  was highly significant,  $p < 0.001$  was extremely significant.

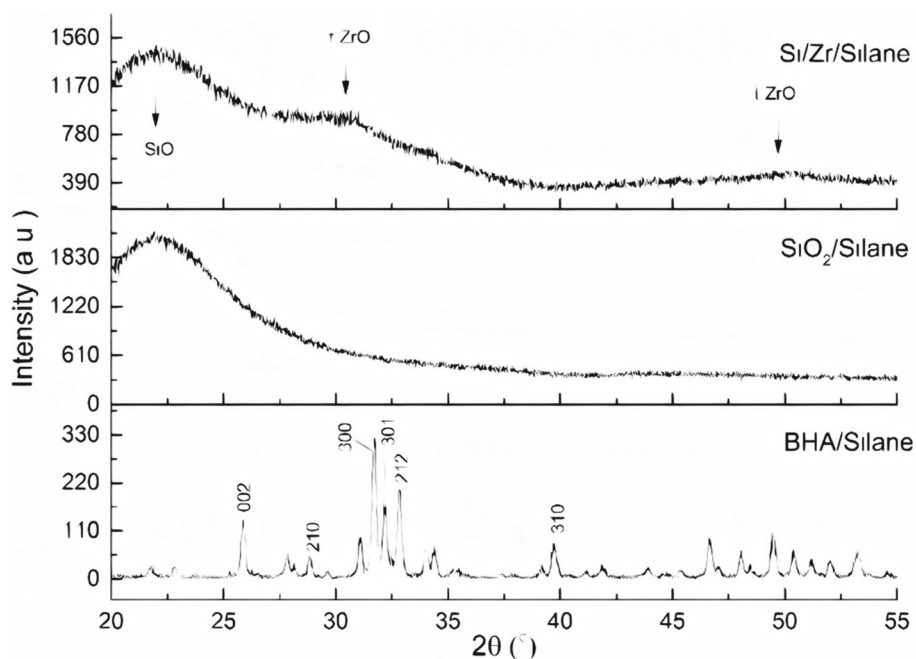
## 3 Results and Discussion

### 3.1 Evaluation of Reinforced Fillers

The XRD patterns of the BHA/Silane,  $\text{SiO}_2$ /Silane, and Si/Zr/Silane reinforced fillers were shown in Fig. 1.

According to the results, the BHA/Silane, and  $\text{SiO}_2$ /Silane were found to be compatible with ICDD (International Centre for Diffraction Data) PDF Card No. 9–432 and No. 029–0085 [31, 32]. The XRD patterns of BHA/Silane were revealed that any secondary phases were not formed in the structure.

**Fig. 1** XRD patterns of BHA/Silane, SiO<sub>2</sub>/Silane and Si/Zr/Silane reinforcing fillers



Characteristic peaks of the BHA were shown at  $2\theta = 26^\circ$  (002),  $29^\circ$  (210),  $32^\circ$  (300),  $40^\circ$  (310) and  $46\text{--}54^\circ$  regions. The lattice parameters of BHA/silane were calculated as  $a = 9.420 \text{ \AA}$  and  $c = 6.880 \text{ \AA}$ . Lattice parameters of pure stoichiometric HA crystals are known as  $a = 9.438 \text{ \AA}$  and  $c = 6.882 \text{ \AA}$  in the hexagonal plane [33]. When the lattice parameters of the BHA/Silane were compared with the pure HA, it was found that the crystallite size of the structure was not significantly affected by the silanization. Amorphous SiO<sub>2</sub>/silane has only one characteristic peak at  $2\theta = 23.5^\circ$  region. It can be evaluated that, the amorphous structure of silica was not affected by silanization and the XRD diffraction of the SiO<sub>2</sub>/Silane was found to be compatible with the literature [31, 34–36]. Likewise, Si/Zr/Silane has broad peaks at  $23.5^\circ$  region and also it has two peaks at  $30^\circ$  (101) and  $50^\circ$  (202). The peak at  $23.5^\circ$  which was confirmed the SiO<sub>2</sub> structure in line with the PDF Card No: 029–0085. Moreover, the low-intensity diffraction peaks at  $30^\circ$  (101) and  $50^\circ$  (202) were related to tetragonal ZrO<sub>2</sub> formation as given in PDF Card No: 42–1164 [33, 35]. The Si/Zr/Silane was consisting of 13% by weight tetragonal ZrO<sub>2</sub> that was located in the SiO<sub>2</sub> lattice.

The FTIR spectrums of the silane-treated fillers are given in Fig. 2.

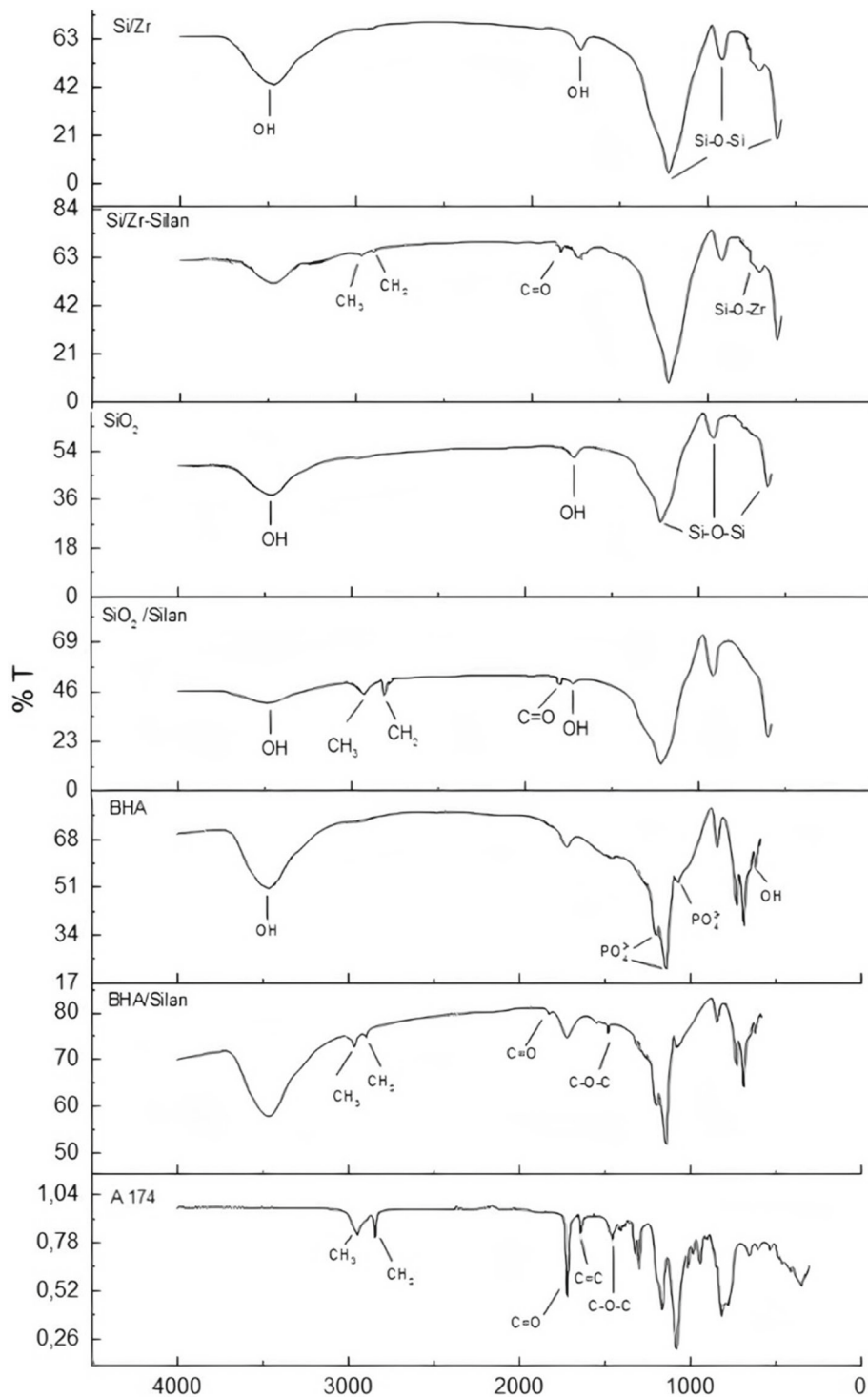
The bands that corresponded to O–P–O bending vibrations occurred at  $570 \text{ cm}^{-1}$  and  $600 \text{ cm}^{-1}$ , and PO stretching vibrations was observed at  $1033 \text{ cm}^{-1}$ ,  $1085 \text{ cm}^{-1}$  and  $960 \text{ cm}^{-1}$ . The stretching mode of the OH<sup>−</sup> group appeared at  $3500 \text{ cm}^{-1}$ . O–H in-plane bending was at  $1651 \text{ cm}^{-1}$ . The characteristic absorption bands of the SiO<sub>2</sub>/Silane and

Si/Zr/Silane were attributed with the asymmetric and symmetric stretching vibrations of the Si–O–Si structure were occurred at  $1100 \text{ cm}^{-1}$ ,  $800 \text{ cm}^{-1}$ , and  $470 \text{ cm}^{-1}$  regions. Also, the peaks at  $3440 \text{ cm}^{-1}$ , and  $1630 \text{ cm}^{-1}$  were related to the –OH groups on the silica surface. Apart from SiO<sub>2</sub>/Silane, Si/Zr/Silane had an absorption at  $745 \text{ cm}^{-1}$ , which was related to the bending vibrations of zirconia (Zr–O–Zr). The bands of 3-MPTMS in silanized fillers were appeared at  $1720 \text{ cm}^{-1}$  for C = O, at  $2900 \text{ cm}^{-1}$  for –CH<sub>3</sub>, at  $2800 \text{ cm}^{-1}$  for –CH<sub>2</sub>, at  $1320 \text{ cm}^{-1}$  for C–O–C, and at  $790\text{--}1100 \text{ cm}^{-1}$  for Si–O–C vibrations. A decrease in the intensity of those peaks was proving the filler modification with A174.

The XPS spectra on the surface of the BHA/Silane, SiO<sub>2</sub>/Silane, and Si/Zr/Silane are given in Fig. 3.

The XPS spectrum of the BHA/Silane contains the Ca (2p),  $346.5 \text{ eV}$ , Ca (2s),  $451 \text{ eV}$ , O (1s),  $531 \text{ eV}$ , P (2p),  $132.5 \text{ eV}$ , Si (2s),  $151.2 \text{ eV}$  and C (1s),  $284.6 \text{ eV}$ . In the literature, the binding energy (BE) of Si (2s) was found  $152.4 \text{ eV}$  in the BHA/Silane structure. This small shift ( $1.2 \text{ eV}$ ) was related to the adjacent P atoms in the P–O–Si bonding which was formed by the filler modification with the 3-MPTMS. Similarly, the BE of P (2p) has a small increase,  $0.5 \text{ eV}$ , when compared with the pure HA [37]. This increase has supported the bonding between BHA and silane structures. The spectrum of the SiO<sub>2</sub>/Silane fillers basically includes Si (2s, 2p), C (1s) and O (1s, 2s) splits. The BE of Si (2p),  $103.6 \text{ eV}$ , O (1s),  $533.6 \text{ eV}$  and C (1s),  $284.6 \text{ eV}$ , respectively. The BE of Si (2p) was shifted to  $0.1 \text{ eV}$  in the SiO<sub>2</sub>/Silane structure compared with the pure SiO<sub>2</sub> [38]. The Si (2p) peak split which has higher binding energy compared with the pure SiO<sub>2</sub> and the existence of C (1s) peak, was

**Fig. 2** FTIR spectrum of silanized and unsilanized reinforcing fillers



confirmed the formation of silica-silane bonding by the A174 modification [39, 40]. The XPS spectrum of the Si/Zr/Silane contains Si (2 s, 2p), C (1 s), Zr (3 s, 3p, 4p, d5), and O (1 s). The binding energies of Zr (3d) at 182.2 eV and, O (1 s) at 532.5 eV were in agreement with the ZrO<sub>2</sub> in the structure. Also, Si (2 s) at 151.2 eV that is supported the formation of P-O-Si bonding and Si (2p) at 102.3 eV, were in agreement

with Si–O–Zr binding between SiO<sub>2</sub>/ZrO<sub>2</sub> mixed oxide and silane structures [41]. Moreover, the higher binding energy of Zr (3d) than pure ZrO<sub>2</sub> (0.5 eV) were indicated the formation of SiO<sub>2</sub>/ZrO<sub>2</sub>.

The TGA thermograms of the unsilanized and silanized fillers are given in Fig. 4.

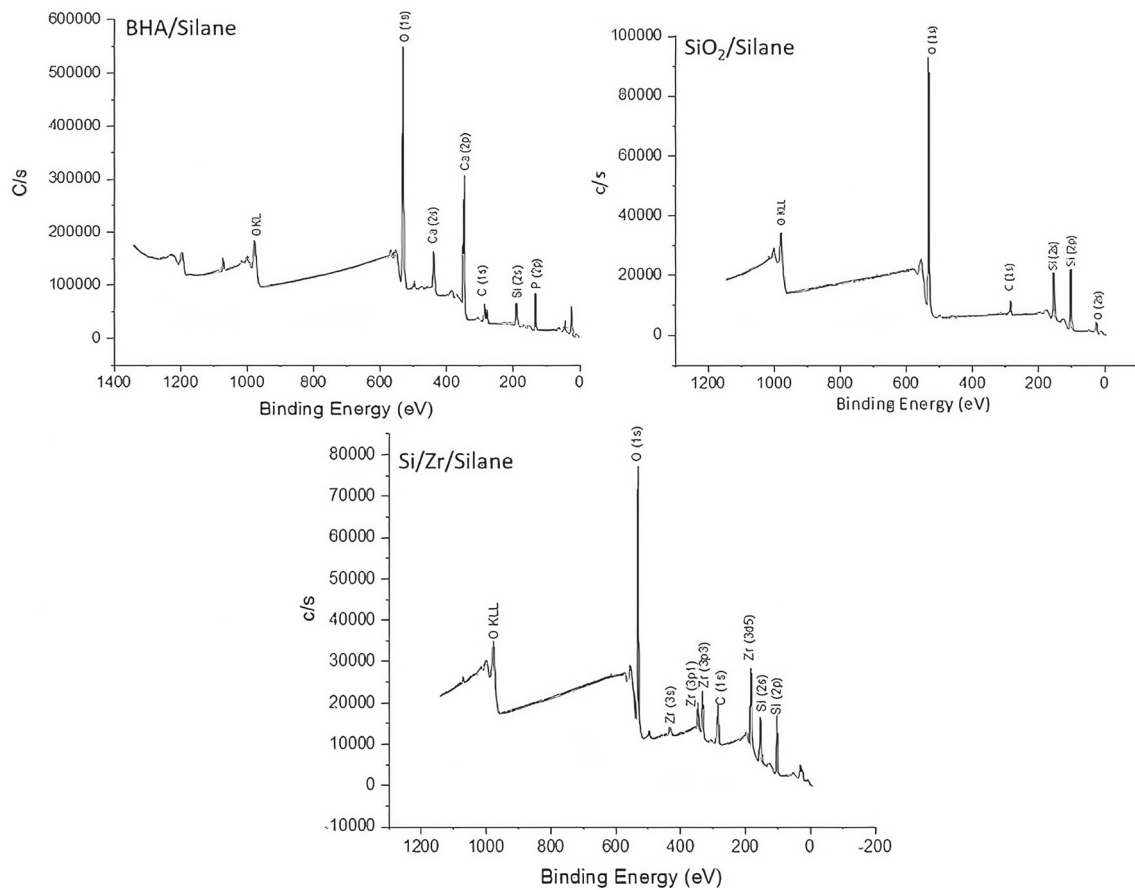


**Fig. 3** XPS spectra of BHA/Silane, SiO<sub>2</sub>/Silane, and Si/Zr/Silane reinforcing fillers

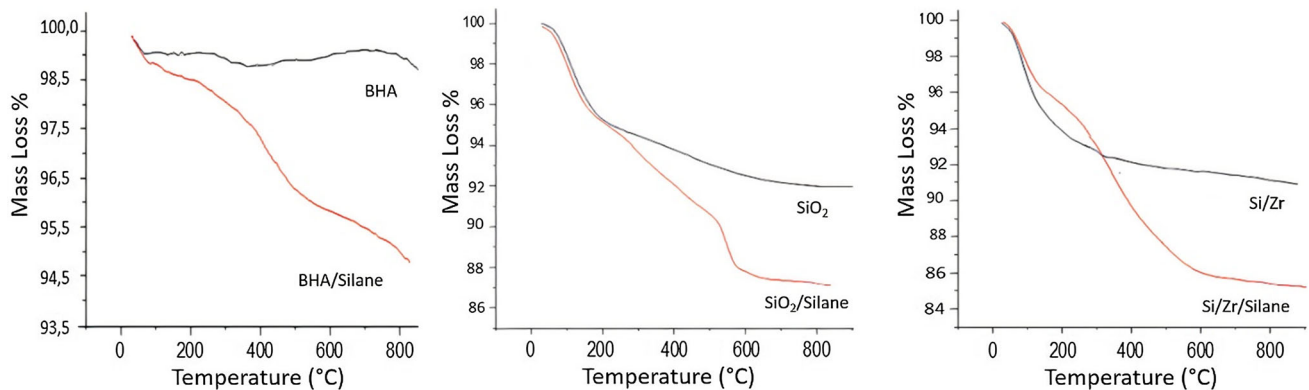


**Fig. 4** TGA thermograms of silanized and unsilanized reinforcing fillers

The results showed that the degradation behavior below 300 °C was similar for both unmodified and modified reinforced fillers, except that the unmodified showed earlier water evaporation than the modified due to the introduction of the hydrophobic 3-MPTMS units [42]. No abrupt change in weight was evident for the modified fillers around 190 °C, which corresponds to the A174 boiling point, confirming their strong chemical bond on the fillers. The degradation behaviors at above 300 °C, however, were quite different for

both cases. The modified fillers lost more of their weight than did the unmodified fillers in the temperature range of 300–700 °C. This difference arose from the degradation of the 3-MPTMS units bound to the fillers. From the difference between the two samples at 600–700 °C, the amount of the 3-MPTMS introduced to fillers was determined approximately 8% (wt.) of the total filler, and the weight loss was calculated about 6% (wt.) after the thermal degradation. This loss was related to the organic units presented in the 3-MPTMS. The

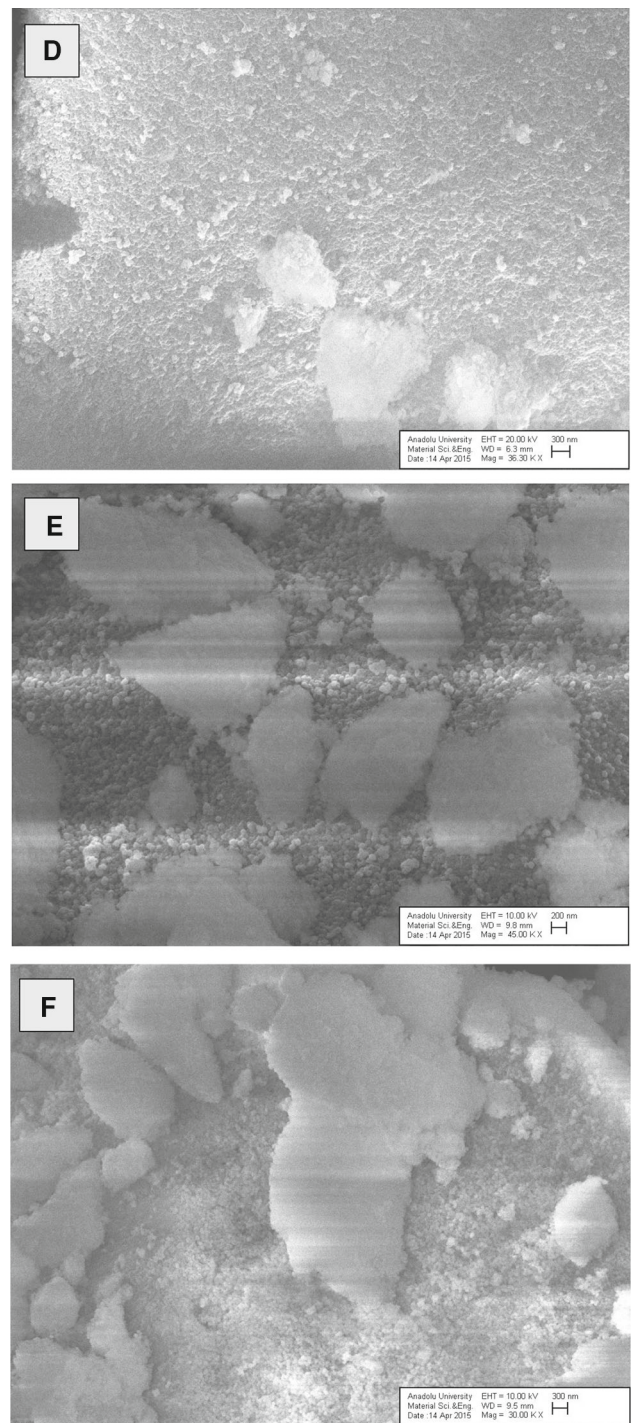
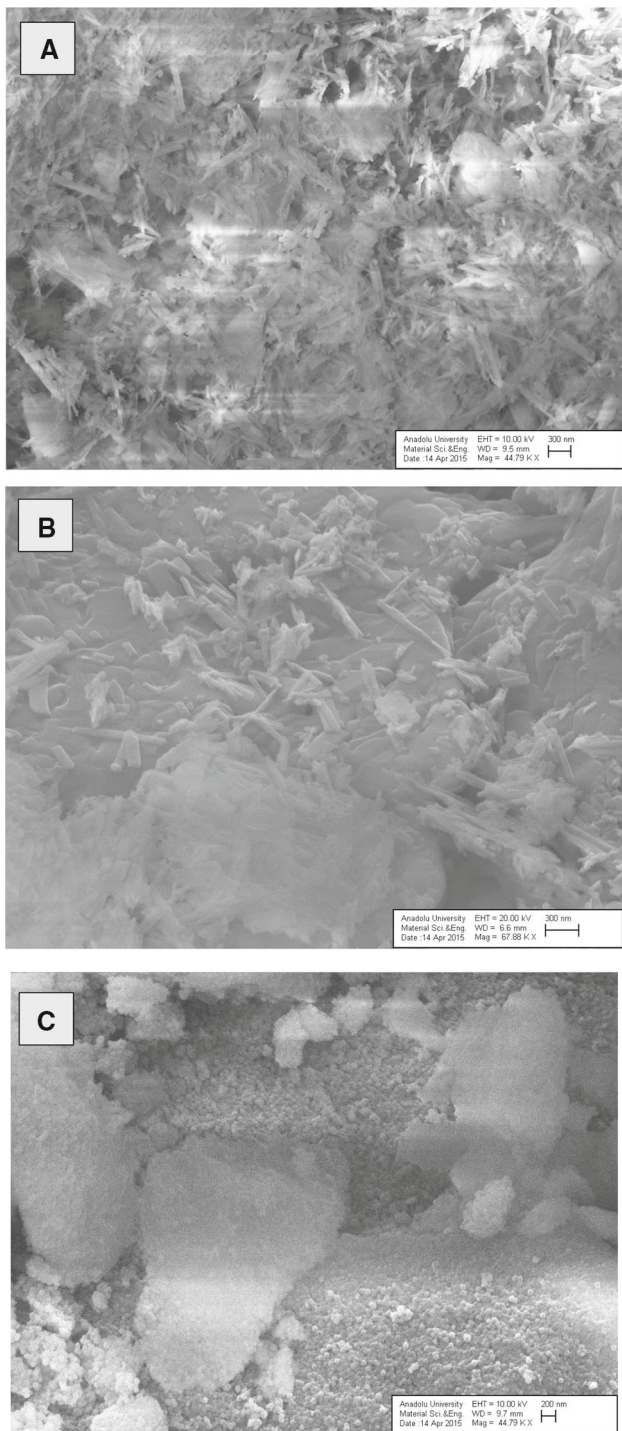


**Fig. 5** SEM images of reinforcing fillers: **A** BHA **B** BHA/Silane **C** SiO<sub>2</sub> **D** SiO<sub>2</sub>/Silane **(E)** Si/Zr **(F)** Si/Zr/Silane

**Fig. 5** continued

weight loss was found at 5.8% (wt.) for the BHA/Silane and, 6% (wt.) for the SiO<sub>2</sub>/Silane and Si/Zr/Silane, respectively. Those results were verified that the experimental findings were compatible with the theoretical calculations. The SEM images of the fillers are given in Fig. 5.

The SEM images of the BHA and BHA/Silane were revealed that the particles had rod shapes and similar dimensions with hydroxyapatite particles in the tooth enamel (25–100 nm diameter 25–100 nm diameter and 100 nm–100 μm dimension along c-axis and 100 nm–100 μm dimension along c-axis) [43]. However, due to the BHA and BHA/Silane particles were not separated

**Table 2** The particle size and surface area values of the unsilanized and silanized fillers

	BHA	BHA/Silane	SiO <sub>2</sub>	SiO <sub>2</sub> /Silane	Si/Zr	Si/Zr/Silane
Particle Size (nm)*	300	300	≤ 300	≤ 300	≤ 2000	≤ 1000
Particle Size (nm)**	235.1	229.8	231.8	154.4	374.9	354
Surface area (m <sup>2</sup> /g)	1.145	30.26	47.15	52.45	56.86	56.86

\*Particle size measurements with SEM, \*\*Particle size measurements with Zeta-Sizer

with exact boundaries from each other, certain particle sizes could not be determined. Nevertheless, it could be said that the mean particle size was under 300 nm for the BHA ceramics. The SEM images of the BHA/Silane samples were also showed that the 3-MPTMS was heterogeneously distributed on the BHA surface and the particle size of the ceramics was decreased with the silanization as was expected. The decrease of the particle size was a result of the lower agglomeration tendency of the BHA/Silane particles. The particle shapes of the SiO<sub>2</sub> and SiO<sub>2</sub>/Silane were determined as spherical from the SEM images. The particle size of the SiO<sub>2</sub>/Silane was found to be lower than the SiO<sub>2</sub> in accordance with the lower agglomeration tendency. However, the 3-MPTMS distribution on the silica surface was not determined due to the similar morphology of the MPTMS and silica. Distinctly from other filler the Si/Zr and Si/Zr/Silane were found to be distributed as clusters. The contribution of the 3-MPTMS compound into the Si/Zr lattice was decreased the mean particle size of the Si/Zr/Silane fillers and it was also found that the Si/Zr/Silane particles were distributed as homogeneously. The particle size of the Si/Zr and Si/Zr/Silane was determined as ≤ 2 μm, and ≤ 1 μm, respectively. However, the 3-MPTMS distribution on the surface could not be determined due to the similar morphology of the MPTMS and Si/Zr nanoclusters.

The particle size and surface area measurements of the silanized and unsilanized fillers are given in Table 2 and the particle size distribution of the fillers is given in Fig. 6.

The particle size measurements of the BHA, BHA/Silane SiO<sub>2</sub>, and SiO<sub>2</sub>/Silane with Zeta Sizer were found to be compatible with the SEM results. From the results, it was seen that modification with the 3-MPTMS was decreased the mean particle size of the fillers due to the lower agglomeration tendency. The particle size of the BHA, BHA/Silane SiO<sub>2</sub>, and SiO<sub>2</sub>/Silane was measured as 235.1 nm, 229.8 nm, 231.8 nm and 154.4 nm, respectively. Also, the surface area measurements of the BHA, BHA/Silane SiO<sub>2</sub>, and SiO<sub>2</sub>/Silane were found to be 1.145 m<sup>2</sup>/g, 30.26 m<sup>2</sup>/g, 47.15 m<sup>2</sup>/g and 52.45 m<sup>2</sup>/g. The measurements have also confirmed the decrease of the particle size and agglomeration of the silanized fillers. Unlike the BHA/Silane and SiO<sub>2</sub>/Silane, silanization of the Si/Zr clusters was not affected the agglomeration tendency of the particles. The mean particle size of the Si/Zr and Si/Zr/Silane was measured as 374.9 nm and 354 nm,

respectively. The surface area values of both samples were measured as 56.86 m<sup>2</sup>/g in accordance with the Zeta Sizer measurements. In literature, the agglomeration tendency of the BHA was reported in the form of clusters. Moreover, the particle size distribution and surface area (m<sup>2</sup>/g) are determinative for the occurrence of chemical reactions [44]. However, the silanization of the BHA and SiO<sub>2</sub> was improved the particle size distribution and surface area. As it was seen in Fig. 6 silanization was resulted with the more narrow particle size distribution. These results were also compatible with our previous studies that report the agglomeration tendency of silanized particles was much less than unsilanized [20]. On the other hand, the silanization showed no effect on the Si/Zr nanocluster particle size distribution.

## 3.2 Evaluation of Dental Composites

### 3.2.1 Evaluation of Mechanical Properties

Restorative materials and teeth are generally subjected to both compressive and flexural loads, so flexural and compressive strength tests are very important to test and determine the mechanical properties of materials. The compressive strength has an important role in the chewing process since several of the masticatory forces are of a compressive nature. In addition, a material's fracture-related properties are usually determined by flexural strength testing and are especially important if the material is used for Class I, II, or IV cavities, which are usually subjected to high loads [45]. The higher compressive and flexural strengths of the restoration materials, used for posterior restorations, are protected the materials as well as tooth structure against fracture. The ISO 4049 classifies dental polymer-based restorative materials into 2 types: Type I is the material claimed by the manufacturer to be suitable for restorations involving occlusal surfaces, and Type II is all other polymer-based filling and restorative materials. The minimum flexural strength requirement for Type I is 80 MPa and 50 MPa for Type II [46, 47]. Even though the flexural strength of the materials is specified with the ISO standards, there are any exact values for other properties of the composites such as compressive strength, angular compressive strength, elasticity modulus, or Vicker's hardness. The ideal value should be similar to that of tooth structure so that the restoration could have similar deformation with



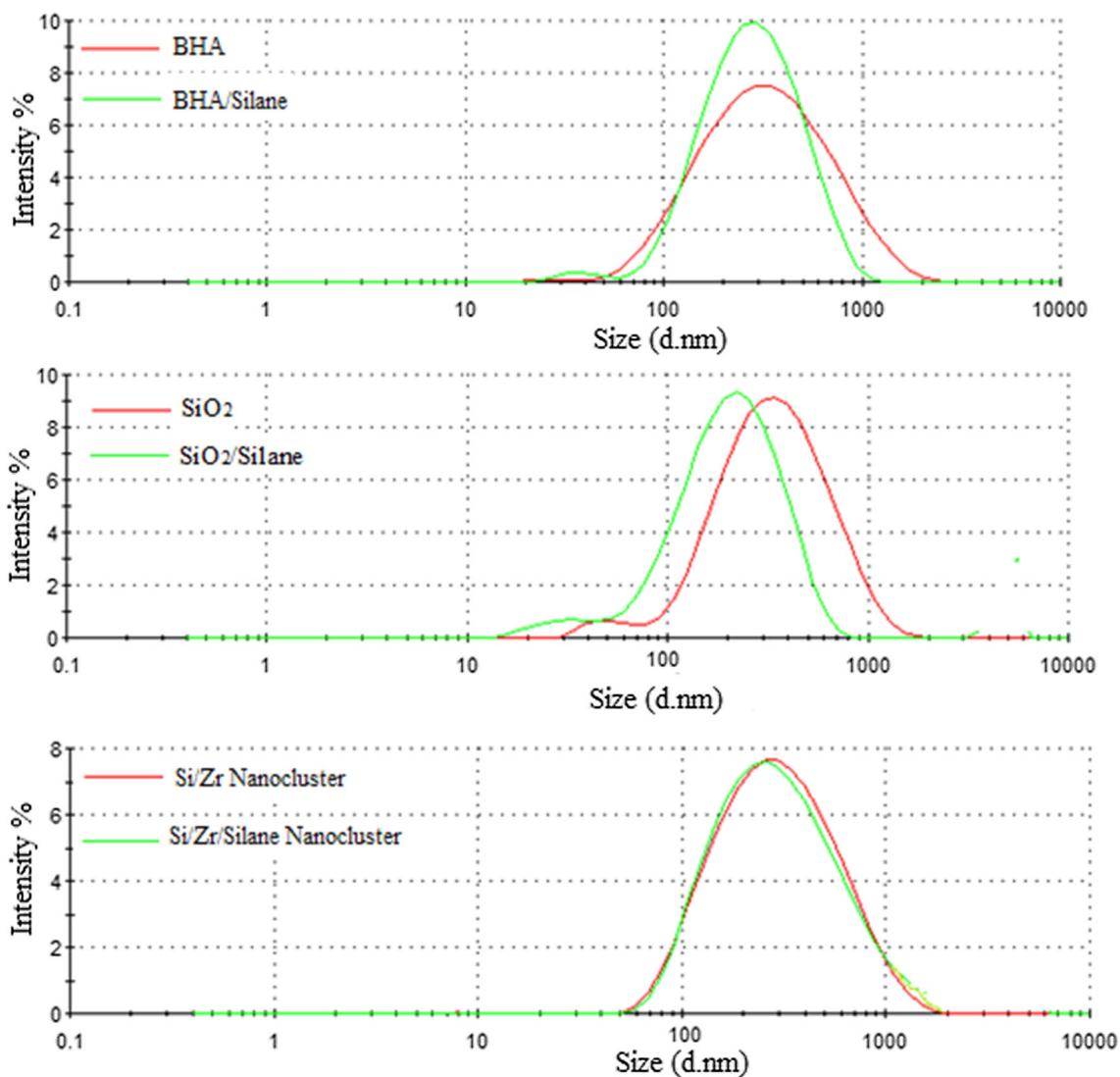


Fig. 6 Mean particle size distribution of the fillers: BHA, BHA/Silane, SiO<sub>2</sub>, SiO<sub>2</sub>/Silane, Si/Zr, and Si/Zr/Silane

Table 3 Mechanical properties of composite resin and BHA filled composite

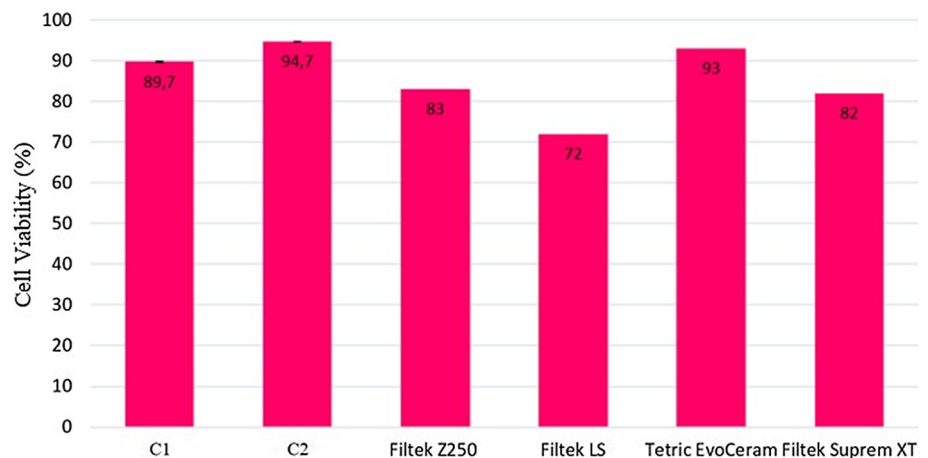
Sample	CS (MPa) <sup>a</sup>	FS (MPa) <sup>a</sup>	E (GPa)	VH (HV)
C1	219.52 ± 7.56	126.71 ± 7.00	12.5 ± 1.3	52.9 ± 0.46
C2	195.54 ± 33.16	103.16 ± 8.01	8.70 ± 0.6	58.0 ± 0.27

the surrounding tooth structure under load. CS, FS, and HV values of the experimental dental restoratives are given in Table 3.

The results showed that all the composites had a flexural strength higher than 80 MPa, so C1 and C2 should be categorized as Type I material. The addition of the BHA/Silane into the composite was decreased the CS ( $p > 0.005$ ), FS ( $p < 0.001$ ), and E ( $p < 0.001$ ) except the HV ( $p < 0.001$ ) as was expected. The decrease of the CS was not significantly different. On the contrary, the increase of HV and the decrease of FS and E were extremely significant differences for C1

and C2. The BHA/Silane addition caused a small increase of VH for C2 composites. The higher VH values were signified that the C2 composite had better properties in the scope of the grinding and polishing. Labella et al. reported that using silanized HA can be improved the FS of Bis-GMA-based dental composites [48]. Additionally, Santos et al. were revealed that silanized HA addition has no effect on the FS of the composites [7]. Leitune et al. were also found that the flexural strength values of the model dental adhesives were shown significant differences between the experimental groups and the control group (HA0%) [49]. Contrariwise

**Fig. 7** Cell viability (%) of experimental, and commercial dental restorative materials



to their findings, this study was showed that silanized BHA addition significantly decrease the FS values of the composites. However, 103.16 MPa values can be still enough to meet the expectations of the ISO 4049 specifications.

The nanosphere agglomerates possibly provide resistance against the diffusion and degradation of the material. According to the literature the surface microhardness of the HA samples may also be enhanced due to the presence of functionalized silane groups on HA nanospheres, which are suggested to lower the capacity of water sorption and prolong bond durability [50]. However, in our study microhardness of the composites were not affected to the addition of BHA. Therefore, it can be imply that HA addition would not be effect of water sorption and prolong bond durability of the dental composites.

### 3.2.2 Evaluation of Biological Properties

According to the ISO 10993–5:2009, samples with cell viability below 70% are considered cytotoxic [51]. From the cytotoxicity tests, the cell viability of C1 and C2 composites were determined as 89.7% and 94.7%, respectively, and their cell viability values were higher than 70% as defined by the ISO 10993–5: 2009 standard. The column graph of (%) cell viability of experimental (C1, C2) and commercial composites (FiltekZ250, Filtek LS, Tetric EvoCeram, Filtek Suprem XT) are given in Fig. 7.

## 4 Conclusion

The present study showed that incorporating the HA into dental composite structures does not reduce the mechanical properties of composites. Moreover, it is improved cell viability and may allow the release of calcium and phosphate ions and remineralization of damaged tissues at the beginning

of the lesions. Although FS was decreased with the addition of HA, the values of flexural strength have still met the requirements in ISO 4049 for posterior restorations. Therefore, the novel biomimetic hydroxyapatite could be capable and promising filler for fabricating dental resin composites with good mechanical properties and potential bioactivity.

**Acknowledgements** This study was financially supported by Yildiz Technical University, Scientific Research Projects Coordination Department within the scope of the Project Numbers 2015-07-02-KAP02 and 2014-07-02-DOP04. The authors also wish to acknowledge Prof. Dr. Gamze Torun Köse, Assoc. Prof. Tülin Şahin, Assoc. Prof. Serap Acar Derman for particle size measurement, and Ms. Görkem Cemali for their meaningful discussion and help during the research.

## References

1. Yadav, K.; Prakash, S.: Dental caries: a review. *Asian J. Biomed. Pharmac. Sci.* **6**, 01 (2016)
2. Pitts, N.B.; Zero, D.T.; Marsh, P.D.; Ekstrand, K.; Weintraub, J.A.; Ramos-Gomez, F.; Tagami, J.; Twetman, S.; Tsakos, G.; Ismail, A.: Dental caries. *Nat. Rev. Dis. Primers.* **3**, 17030 (2017)
3. AlJehani, Y.A.; Baskaradoss, J.K.; Geevarghese, A.; AlShehry, M.A.: Current trends in aesthetic dentistry. *Health* **6**, 1941 (2014)
4. Fugolin, A.; Pfeifer, C.: New resins for dental composites. *J. Dent. Res.* **96**, 1085–1091 (2017)
5. Arsecularatne, J.; Chung, N.; Hoffman, M.: An in vitro study of the wear behaviour of dental composites. *Biosurf. Biotribol.* **2**, 102–113 (2016)
6. Aljabo, A.; Neel, E.A.A.; Knowles, J.C.; Young, A.M.: Development of dental composites with reactive fillers that promote precipitation of antibacterial-hydroxyapatite layers. *Mater. Sci. Eng., C* **60**, 285–292 (2016)
7. Santos, C.; Luklinska, Z.; Clarke, R.; Davy, K.: Hydroxyapatite as a filler for dental composite materials: mechanical properties and in vitro bioactivity of composites. *J. Mater. Sci. - Mater. Med.* **12**, 565–573 (2001)
8. Pepla, E.; Besharat, L.K.; Palaia, G.; Tenore, G.; Migliau, G.: Nano-hydroxyapatite and its applications in preventive, restorative and regenerative dentistry: a review of literature. *Ann. Stomatol.* **5**, 108 (2014)
9. Calabrese, L.; Fabiano, F.; Currò, M.; Borsellino, C.; Bonaccorsi, L.; Fabiano, V.; Ientile, R.; Proverbio, E.: Hydroxyapatite

- whiskers based resin composite versus commercial dental composites: mechanical and biocompatibility characterization. *Adv. Mater. Sci. Eng.* **2016**, 1–9 (2016)
10. Liu, F.; Sun, B.; Jiang, X.; Aldeyab, S.S.; Zhang, Q.; Zhu, M.: Mechanical properties of dental resin/composite containing urchin-like hydroxyapatite. *Dent. Mater.* **30**, 1358–1368 (2014)
  11. Wu, Y.R.; Chang, C.W.; Chang, K.C.; Lin, D.J.; Ko, C.L.; Wu, H.Y.; Chen, W.C.: Effect of micro-/nano-hybrid hydroxyapatite rod reinforcement in composite resins on strength through thermal cycling. *Polym. Compos.* **40**, 3703–3710 (2019)
  12. Pajor, K.; Pajchel, L.; Kolmas, J.: Hydroxyapatite and fluorapatite in conservative dentistry and oral implantology—a review. *Materials* **12**, 2683 (2019)
  13. Scribante, A.; Dermenaki Farahani, M.R.; Marino, G.; Matera, C.; Rodriguez y Baena, R.; Lanteri, V.; Butera, A.: Biomimetic effect of nano-hydroxyapatite in demineralized enamel before orthodontic bonding of brackets and attachments: Visual, adhesion strength, and hardness in in vitro tests. *BioMed Res. Int.* **2020**, 1–9 (2020)
  14. Memarpour, M.; Shafiei, F.; Rafiee, A.; Soltani, M.; Dashti, M.H.: Effect of hydroxyapatite nanoparticles on enamel remineralization and estimation of fissure sealant bond strength to remineralized tooth surfaces: an in vitro study. *BMC Oral Health* **19**, 1–14 (2019)
  15. Craig, B.D.: Fillers and composite materials with zirconia and silica nanoparticles, ed's eds.: Google Patents (2014).
  16. Razali, R.; Rahim, N.; Zainol, I.; Sharif, A.: Preparation of Dental Composite Using Hydroxyapatite from Natural Sources and Silica. IOP Publishing, Bristol (2018)
  17. Ozmen, M.; Akin, I.; Marsoglu, M.: Production and characterization of hydroxyapatite-zirconia composites. *High Temp. Mater. Processes* **31(6)**, 749–753 (2012)
  18. Lung, C.Y.K.; Matinlinna, J.P.: Aspects of silane coupling agents and surface conditioning in dentistry: an overview. *Dent. Mater.* **28**, 467–477 (2012)
  19. Kango, S.; Kalia, S.; Celli, A.; Njuguna, J.; Habibi, Y.; Kumar, R.: Surface modification of inorganic nanoparticles for development of organic-inorganic nanocomposites—A review. *Prog. Polym. Sci.* **38**, 1232–1261 (2013)
  20. Aydınoglu, A.; Yoruç, A.B.H.: Effects of silane-modified fillers on properties of dental composite resin. *Mater. Sci. Eng., C* **79**, 382–389 (2017)
  21. Amend, S.; Frankenberger, R.; Lucker, S.; Domann, E.; Krämer, N.: Secondary caries formation with a two-species biofilm artificial mouth. *Dent. Mater.* **34**, 786–796 (2018)
  22. Jacob, M.: Biofilms, a new approach to the microbiology of dental plaque. *Odontology* **94**, 1–9 (2006)
  23. Melo, M.A.S.; Cheng, L.; Weir, M.D.; Hsia, R.C.; Rodrigues, L.K.; Xu, H.H.: Novel dental adhesive containing antibacterial agents and calcium phosphate nanoparticles. *J. Biomed. Mater. Res. B Appl. Biomater.* **101**, 620–629 (2013)
  24. Ribeiro, M.R.d.C.: Study of nanostructured hydroxyapatite based surfaces to prevent biofilm formation associated to implant infections. Thesis (2011)
  25. Çalışkan, F.V.: Pedodontide kullanılan farklı dental materyallerin yüzey özellikleri and mikrosertlikleri ile in situ oluşan biofilm tabakasının yapısı arasındaki ilişkinin incelenmesi. Thesis (2014)
  26. Hazar Yoruç, A.; Karakaş, A.; Ayas, E.; Koyun, A.: Effect of precipitation method on properties of hydroxyapatite powders. *Acta Phys. Pol. A* **123**, 371–373 (2013)
  27. Tas, A.C.: Synthesis of biomimetic Ca-hydroxyapatite powders at 37 C in synthetic body fluids. *Biomaterials* **21**, 1429–1438 (2000)
  28. Yoruç, A.B.H.; Aydınoglu, A.: The precursors effects on biomimetic hydroxyapatite ceramic powders. *Mater. Sci. Eng., C* **75**, 934–946 (2017)
  29. Lia, Z.C.; White, S.N.: Mechanical properties of dental luting cements. *J. Prosthet. Dent.* **81**, 597–609 (1999)
  30. Flury, S.; Hayoz, S.; Peutzfeldt, A.; Hüsler, J.; Lussi, A.: Depth of cure of resin composites: is the ISO 4049 method suitable for bulk fill materials? *Dent. Mater.* **28**, 521–528 (2012)
  31. Devi, R.R.; Maji, T.K.: Interfacial effect of surface modified TiO<sub>2</sub> and SiO<sub>2</sub> nanoparticles reinforcement in the properties of wood polymer clay nanocomposites. *J. Taiwan Inst. Chem. Eng.* **44**, 505–514 (2013)
  32. Sadat-Shojai, M.; Atai, M.; Nodehi, A.; Khanlar, L.N.: Hydroxyapatite nanorods as novel fillers for improving the properties of dental adhesives: Synthesis and application. *Dent. Mater.* **26**, 471–482 (2010)
  33. Ko, J.-B.; Lee, S.W.; Kim, D.E.; Kim, Y.U.; Li, G.; Lee, S.G.; Chang, T.-S.; Kim, D.; Joo, Y.L.: Fabrication of SiO<sub>2</sub>-ZrO<sub>2</sub> composite fiber mats via electrospinning. *J. Porous Mater.* **13**, 325–330 (2006)
  34. Aquino, F.T.; Pereira, R.R.; Ferrari, J.L.; Ribeiro, S.J.L.; Ferrier, A.; Goldner, P.; Gonçalves, R.R.: Unusual broadening of the NIR luminescence of Er<sup>3+</sup>-doped Nb<sub>2</sub>O<sub>5</sub> nanocrystals embedded in silica host: Preparation and their structural and spectroscopic study for photonics applications. *Mater. Chem. Phys.* **147**, 751–760 (2014)
  35. Ferrari, J.L.; Lima, K.O.; Maia, L.J.; Ribeiro, S.J.; Gonçalves, R.R.: Structural and spectroscopic properties of luminescent Er<sup>3+</sup>-doped SiO<sub>2</sub>-Ta<sub>2</sub>O<sub>5</sub> nanocomposites. *J. Am. Ceram. Soc.* **94**, 1230–1237 (2011)
  36. Dai, Y.M.; Hsieh, J.H.; Chen, C.C.: Transesterification of soybean oil to biodiesel catalyzed by waste silicone solid base catalyst. *J. Chin. Chem. Soc.* **61**, 803–808 (2014)
  37. Raikar, G.N.; Ong, J.L.; Lucas, L.C.: Hydroxyapatite characterized by XPS. *Surf. Sci. Spectra* **4**, 9–13 (1996)
  38. Zhang, K.; Wu, W.; Guo, K.; Chen, J.-F.; Zhang, P.-Y.: Magnetic polymer enhanced hybrid capsules prepared from a novel Pickering emulsion polymerization and their application in controlled drug release. *Colloids Surf., A* **349**, 110–116 (2009)
  39. Cui, X.; Zhong, S.; Yan, J.; Wang, C.; Zhang, H.; Wang, H.: Synthesis and characterization of core-shell SiO<sub>2</sub>-fluorinated polyacrylate nanocomposite latex particles containing fluorine in the shell. *Colloids Surf., A* **360**, 41–46 (2010)
  40. Guittet, M.; Crocombette, J.; Gautier-Soyer, M.: Bonding and XPS chemical shifts in ZrSiO<sub>4</sub> versus SiO<sub>2</sub> and ZrO<sub>2</sub>: charge transfer and electrostatic effects. *Phys. Rev. B* **63**, 125117 (2001)
  41. Dupraz, A.; De Wijn, J.; vd Meer, S.; De Groot, K.: "Characterization of silane-treated hydroxyapatite powders for use as filler in biodegradable composites. *J. Biomed. Mater. Res. Official J. Soc. Biomater. Japanese Soc. Biomater.* **30**, 231–238 (1996)
  42. Ham, M.J.; Kim, Y.H.: Property modulation of poly (N-isopropylacrylamide) hydrogels by incorporation of modified silica. *Polym. Eng. Sci.* **48**, 2439–2445 (2008)
  43. Cao, Y.; Mei, M.L.; Li, Q.-L.; Lo, E.C.M.; Chu, C.H.: Enamel prism-like tissue regeneration using enamel matrix derivative. *J. Dent.* **42**, 1535–1542 (2014)
  44. Lelli, M.; Putignano, A.; Marchetti, M.; Foltran, I.; Mangani, F.; Procaccini, M.; Roveri, N.; Orsini, G.: Remineralization and repair of enamel surface by biomimetic Zn-carbonate hydroxyapatite containing toothpaste: a comparative in vivo study. *Front. Physiol.* **5**, 333 (2014)
  45. Didem, A.; Yalcin, G.: Comparative mechanical properties of bulk-fill resins. *Open J. Comp. Mater.* (2014).
  46. Goracci, C.; Cadenaro, M.; Fontanive, L.; Giangrosso, G.; Juloski, J.; Vichi, A.; Ferrari, M.: Polymerization efficiency and flexural strength of low-stress restorative composites. *Dent. Mater.* **30**, 688–694 (2014)
  47. Lu, H.; Lee, Y.-K.; Oguri, M.; Powers, J.M.: Properties of a dental resin composite with a spherical inorganic filler. *Oper. Dent.* **31**, 734–740 (2006)
  48. Labella, R.; Braden, M.; Deb, S.: Novel hydroxyapatite-based dental composites. *Biomaterials* **15**, 1197–1200 (1994)



49. Leitune, V.C.B.; Collares, F.M.; Trommer, R.M.; Andrioli, D.G.; Bergmann, C.P.; Samuel, S.M.W.: The addition of nanostructured hydroxyapatite to an experimental adhesive resin. *J. Dent.* **41**, 321–327 (2013)
50. Dorozhkin, S.V.: Chapter 7: Nanodimensional and Nanocrystalline Calcium Orthophosphates, ed. *Tissue Regeneration: Where Nano-Structure Meets Biology*. World Scientific, pp. 219–341 (2014).
51. Farsalinos, K.E.; Romagna, G.; Alliffranchini, E.; Ripamonti, E.; Bocchietto, E.; Todeschi, S.; Tsiapras, D.; Kyrzopoulos, S.; Voudris, V.: Comparison of the cytotoxic potential of cigarette smoke and electronic cigarette vapour extract on cultured myocardial cells. *Int. J. Environ. Res. Public Health* **10**, 5146–5162 (2013)

